Influence of the mobility of Pt nanoparticles on the anisotropic etching properties of silicon

Xiaopeng Li[1,2], Yanjun Xiao[3], Chenglin Yan[1], Keya Zhou[3], Stefan L. Schweizer[2], Alexander Sprafke[2],Jung-Ho Lee[3*], Ralf B. Wehrspohn[2,4*]

1. Max-Planck Institute of Microstructure Physics, Weinberg 2, Halle D-06120, Germany
2. Institute of Physics, Martin-Luther-Universität Halle-Wittenberg, Germany
3. Department of Chemical Engineering, Hanyang University, Ansan, Kyounggi 426-791, Korea
4. Fraunhofer Institute for Mechanics of Materials IWM Halle D-06120, Germany

[*] E-mail: jungho@hanyang.ac.kr (J.-H. Lee), Ralf.Wehrspohn@iwmh.fraunhofer.de (R. B. Wehrspohn)

Abstract:

Metal-assisted chemical etching (MaCE) has been shown to be a powerful and cost-effective method for surface nano-texturing and silicon micromachining. Since the motion of a metal catalyst during the etching process determines the etched morphology, understanding the mobility of the metal catalysts would enable precise control of the silicon structuring. Through the investigation of Pt nanoparticle (PtNP)-induced etching of silicon, we find that the Schottky barrier height of the metal-Si contacts strongly influences the charge transfer process during the etching. Consequently, the motion of the PtNPs is affected, which is different from previous understandings based on an electrokinetic model.

Introduction

In the past decade, the fabrication of silicon nanostructures has aroused great interests. Ranging in size from hundreds of micrometers to less than ten nanometers, silicon structures have a broad spectrum of applications, including photovoltaic cells[1], lithium-ion batteries[2], optoelectronics[3], and microelectromechanical systems (MEMS)[4]. With the shrinkage of structural dimensions and the increase of aspect ratio, silicon nano- and micro-structures become more optically[5], electrically[6], and chemically[7] active than bulk silicon, thus improving the corresponding device performance. However, such improvements strongly depend on specific control of both structural morphology and dimension, thus requiring precise and reproducible preparation methods.

Cost-effective wet etching methods, including electrochemical etching (EE)[8,9], and metal-assisted chemical etching (MaCE), have been recently extensively studied[10-11]. EE is able to create deep pores and trenches in the order of a micrometer[8], however the created structures are always restricted to the dimension of space charge region (SCR)[9].

Metal-assisted chemical etching is a solution based high throughput technique which does not require the application of an external bias. It involves two steps: the deposition of metallic nanoparticles (NPs) or thin films on a Si surface, and the subsequent etching of Si in an HF, H_2O_2 and H_2O solution. The metal acts as a catalyst, penetrating deep into the Si substrates[11], while Si in the vicinity of the metal dissolves. Hence, the motion of the metal determines the etching direction. Since the (100) plane has the fewest Si back bonds to break, the etching direction is preferable along the <100> direction[11]. However, if the metal nanoparticles were not densely interconnected, the sparsely distributed metal nanoparticles including Ag[12], Au[13], Pd[14]

and Pt[15], sometimes travel in unexpected directions through the silicon. Especially for Pt and Pd, the etching paths are very wavy. Previously, Peng et al.[16] proposed an electrokinetic model to explain the autonomous motion of AgNPs. The electron flow through NPs is coupled with proton translocation in the fluid, which implies an electrical field capable of introducing electrokinetic effects. This model neglects the influence of the Si-metal contact on charge transfer, and cannot fully explain the mobility of metal catalysts. Furthermore, it was found that Ag and Au catalysts were easier to dissolve in the etchant, and caused a rugged surface for the micromachining of silicon. In contrast, Pt and Pd exhibit better stability against dissolution, and a higher etching speed[17]. It is therefore crucial to investigate the etched morphology by single PtNP, and more importantly to understand the origin of the mobility of the metal NPs. Employing MaCE could therefore benefit the fabrication of complex 2-D and 3-D silicon structures.

Results and discussion

Cz-grown, single-side polished p-type and n-type, single-crystal (100) silicon wafers with two types of resistivities, 1-10 Ω cm (p^-, n^-, moderately doped) and 0.01-0.02 Ω cm (p^+, n^+, highly doped), were used in this study. Sparsely distributed spherical nanoparticles (PtNPs) with diameter 20nm – 200nm, and density ~5×10^8 cm^{-2} were deposited on the Si surface using galvanic displacement by immersing the Si samples into a solution containing 0.5 M HF and 1 mM K_2PtCl_6 shown in Fig. 1(a). The PtNP density slightly increases with the doping level of Si substrates.

Fig. 1(b-d) shows SEM images of the Si samples with various levels of doping etched in HF + H_2O_2 solution. For p^+-Si, the PtNPs drilled vertical macropores with a diameter of d~100 nm into the Si in the <100> direction, while the silicon changed into a uniform and highly porous

structure in the areas not covered by Pt (Fig. 1(b)). In case of p^-- and n^--Si, the etching paths of the PtNPs did not strictly follow the <100> direction (Fig. 1(c)), and the silicon surrounding the etching paths was partially dissolved, turning into non-uniform porous silicon (PSi). The PtNPs deposited on the n^+-Si were not able to form a deep channel. The PtNPs revealed a high mobility near the surface during etching, as shown in Fig. 1(d).

A precise examination of the charge transport process across the etchant-Si-metal interface is critically required to understand the different etching behavior of the various Si substrates shown in Fig. 1(e). When a p-type Si is brought in contact to the etchant, band bending occurs at the Si surface, resulting from equilibration of the Fermi energy level in Si with that of the chemical potential (redox potential) in the etchant[18]. The result of such an equilibration is the formation of an energetic (Schottky) barrier Φ_B^o that inhibits charge transfer at the interface. The band diagram is sketched in Fig. 2(a). After metal NP deposition, the Fermi level $E_F(M)$ is found to be relatively low, near the valence band edge of $E_V(E)$. The conduction and valence band edges ($E_C(M)$ and $E_V(M)$) at the metal NP-Si change their energetic locations according to E_F, while the band edges of $E_C(E)$ and $E_V(E)$ at the etchant-Si interface remain constant[19]. Meanwhile, the local barrier height at the NP-Si interface is lowered to $\Phi_{B,M}$, depending on the value of the metal work function. A low barrier allows for hole-injection through the metal-Si contact, making etching possible. Once etching is initiated, the etchant-facing side of the metal NPs serves as a cathode for hole generation by H_2O_2 reduction, while the silicon-facing side of the NPs acts as an anode for hole injection into the Si surface for dissolution. As a rate-limiting step in a physical scope, either the hole generation at the cathode (cathodic current, j_C), or the hole transport through the metal-Si Schottky barrier for silicon dissolution (anodic current j_A) determines the etched morphology of porous silicon.

Since Pt can decompose H_2O_2 more effectively than Ag, the j_C is greatly enhanced[20], causing excessive silicon dissolution in the vicinity of PtNPs as compared with Ag. However, this cannot fully explain the observed morphological differences while changing the levels and types of substrate doping shown in Fig. 1(e).

We suggest that the anodic current j_A plays a crucial role during the investigated etching process. Contributions to j_A consist normally of diffusion, thermionic emission (TE), or tunneling of holes[9]. We estimate the contribution from the diffusion current to be insignificant due to the blocking effect of the surface energy barrier. TE of holes from the metal over the barrier $\Phi_{B,M}$ into the silicon is known as a dominant process for p^- and n^--Si[9]. In the case of p^+-type Si, heavy doping shifts E_F towards E_{VB}, and reduces $\Phi_{B,M}$ further. Moreover, the SCR width was squeezed and the electrical field magnified in the SCR, allowing the holes to pass the SCR by band-to-band tunneling[18]. It is expected that tunneling leads to higher local currents, and therefore more Si dissolution than TE, thus explaining the PSi structures shown in Fig. 1(b) and (c). In contrast, after the deposition of Pt onto n^+-Si, the $\Phi_{B,M}$ became much higher than that of n^-, p^- and p^+, due to the large work function of Pt[21]. j_A was significantly depressed, and no highly porous structure was produced (see Fig. 1(d)).

In order to validate the hypothesis, OCP and short circuit current were measured (Fig. 2(b-c)) by a potentiostat using Pt wire as counter and reference electrode. The actual Schottky barrier difference $\Phi_{B,M} - \Phi_B^o$ can be extracted from the OCP difference[22]: $\Delta = OCP_{Si/Etchant} - OCP_{Si/metal}$. As the value of Δ increases, the barrier height of $\Phi_{B,M}$ decreases. With the increase of PtNP deposition time, Δ also increases. After 3 min of Pt deposition, Δ is 0.22 V for the highly-doped Si, which is larger than the 0.18 V for the highly-doped Si nearly completely covered with Ag, and the 0.19 V for moderately-doped Si. The short circuit current for highly-doped Si loaded

with PtNPs was 3 times higher than that for moderately-doped Si at the starting point of etching, proving the higher tunneling current over TE. The reduction of OCP and short circuit current was caused either by the degradation of metal-Si contact[23], or the limited diffusion of the etchant.

The mobility difference is also rising due to the difference in j_A. As previously stated, the high catalytic activity of Pt over Ag generates high j_C. In the case of low $\Phi_{B,M}$ at p^+-type Si, j_A arising from tunneling can effectively accept all holes for etching. However, decreasing the p-type doping would increase $\Phi_{B,M}$, as j_A from TE cannot take in the large amount of holes coming from the cathode. The excessive number of holes which accumulate at the NP-Si interface are then able to attack the Si non-(100) crystal planes with a higher density of silicon back bonds, resulting in a non-<100> etching direction. In the extreme case of heavy n-type doping, the surface barrier is high enough that the vertical etching is greatly suppressed, and accumulated holes tend to etch silicon in random horizontal directions.

Conclusions

In summary, we systematically investigated the PtNP induced etching of silicon. The etched morphology of the fabricated PSi and the mobility of the PtNPs show a strong dependence on the Si doping level and type. Such dependence is attributed to the difference of the charge transfer process arising from the various Schottky barrier heights of the metal-Si contact. We believe our model could be generalized not only applying in Pt, but also in Ag, Au, Pd during wet etching, or even the metal nanoparticle assisted dry etching such as W[24] and Au[25]. We have shown that it is critical to select the appropriate metal or metal alloy catalyst with a suitable work function, and a silicon substrate with the right doping level and type, in order to achieve the desired Si nanostructure or microstructure.

References:

1. K. Q. Peng, X. Wang, L. Li, X.-L. Wu, and S.-T. Lee, J. Am. Chem. Soc., **132**, 6872 (2010).

2. M. Ge, J. Rong, X. Fang, and C. Zhou, Nano Lett., **12**, 2318 (2012).

3. R. Yan, D. Hargas, and P. Yang, Nature Photonics, **3**, 569 (2009).

4. J. Sun, D. Cui, Y. Li, L. Zhang, J. Chen, H. Li, and X. Chen, Sens. Actuators B, **141,** 431 (2009).

5. J.-Y. Jung, K. Zhou, H.-D. Um, Z. Guo, S.-W. Jee, K.-T. Park, and J.-H. Lee, Opt. Exp. **36**, 2677 (2011).

6. Y. Cui, Z. Zhong, D. Wang, W. U. Wang, and C.M. Lieber, Nano Lett., **3**, 149 (2003).

7. J. Oh, T.G. Deutsch, H.-C. Yuan, and H. M. Branz, Energy Environ. Sci., **4**, 1690 (2011).

8. T. Geppert, S.L. Schweizer, U. Gösele, and R. B. Wehrspohn, Appl. Phys. A, **84**, 237 (2006).

9. V. Lehmann, Electrochemistry of silicon. Wiley-VCH, Weinheim, 2002.

10. K. Peng, J. Hu, Y. Yan, Y. Wu, H. Fang, Y. Xu, S.-T. Lee, and J. Zhu, Adv. Func. Mater., **16**, 387 (2006).

11. Z. Huang, N. Geyer, P. Werner, J. d. Boor, and U. Gösele, Adv. Mater., **23**, 285 (2011).

12. J. Oh, H.-C. Yuan, and H. M. Branz, Nature Nanotech., **7**, 743 (2012).

13. D. H. Wan, H. L. Chen, S. Y. Chuang, C. C. Yu and Y. C. Lee, J. Phys. Chem. C, **112**, 20567 (2008).

14. M. Lipinski, J. Cichoszewski, R. P. Socha, and T. Piotrowski, Acta Physics Polonica , 116, S117 (2009).

15. K. Tsujino, and M. Matsumura, Electrochem. Solid Stat. Lett. **8**, C193 (2005).

16. K. Peng, A. Lu, R. Zhang, and S.-T. Lee, Adv. Func. Mater., **18**, 3026 (2008).

17. H. Asoh, F. Arai, and S. Ono, Electrochimica Acta **54**, 5142 (2009).

18. W.-K. To, C.-H. Tsang, H-,H. Li, and Z. Huang, Nano Lett. **11**, 5252 (2011).

19. Y. Nakato, H. Yano, S. Nishiura, T. Ueda, and H. Tsubomura, J. Electroanal. Chem. **228**, 97 (1987).

20. C.-L. Lee, K.T. Tsujino, Y. Kanda, S. Ikeda, and M. Matsumura, J. Mater. Chem. **18**, 1015 (2008).

21. S. M. Sze and K.K. Ng, Physics of semiconductor devices; Wiley, NJ, 2007.

22. Z, Huang, N. Geyer, L. F. Liu, M. Y. Li, and P. Zhong, Nanotechnology **21**, 465301(2010).

23. Sharma, P., and Y.-L. Wang, Appl. Phys. Exp. **4**, 025001(2011).

24. W. T. Stacy, E. K. Broadbent, and M. H. Norcott, J. Electrochem. Soc. **132**, 444 (1985).

25. T. James, Y. V. Kalinin, C.-C. Chan, J. S. Randhawa, M. Gaevski, and D. H. Gracias, Nano Lett., **12**, 3437 (2012).

Figure Captions:

Figure 1. SEM images of (a) PtNPs deposited on a Si surface, (b) p^+-Si after etching, (c) p^--Si and n^--Si after etching, and (d) n^+-Si after etching. (a) and (d) are top-view, (b) and (c) are cross-sectional views. (e) A schematic map of porosity vs. doping level of silicon.

Figure 2. (a) Schematic energy band diagram for a particulate-metal/p-Si in the dark. $E_{F,}$ E_C, and E_V are the Fermi level, the bottom of conduction band, and the top of valence band of p-Si, respectively. E(M) and E(E) represent the energy levels of metal-Si and metal-etchant contact, respectively. SCR denotes a space charge region; (b) Time dependence of OCP in p^+-type Si etching with 3 min Pt deposition (red), 1min Pt deposition (green), Ag deposition (blue), and non-treatment (black); (c) Time dependence of short circuit current during etching, p^--Si with Pt deposition (black), p^+ with Pt deposition (red), and Ag deposition (blue).

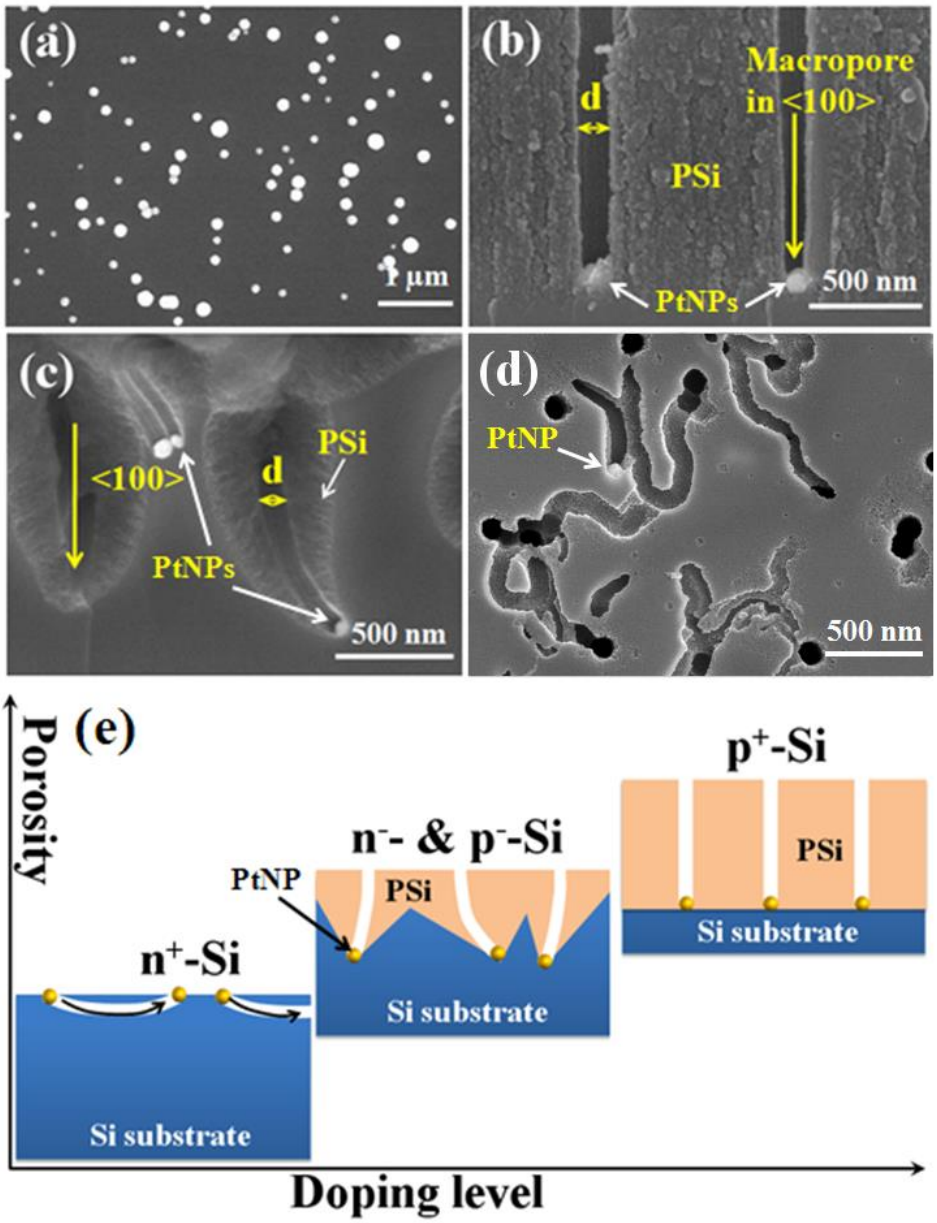
(a)
1 µm
(b)
d
Macropore
in <100>
PSi
PtNPs
500 nm
(c)
<100>
d
PSi
PtNPs
500 nm
(d)
PtNP
500 nm
(e)
Porosity
n⁺-Si
Si substrate
PtNP
n⁻- & p⁻-Si
PSi
Si substrate
p⁺-Si
PSi
Si substrate
Doping level

Fig. 1

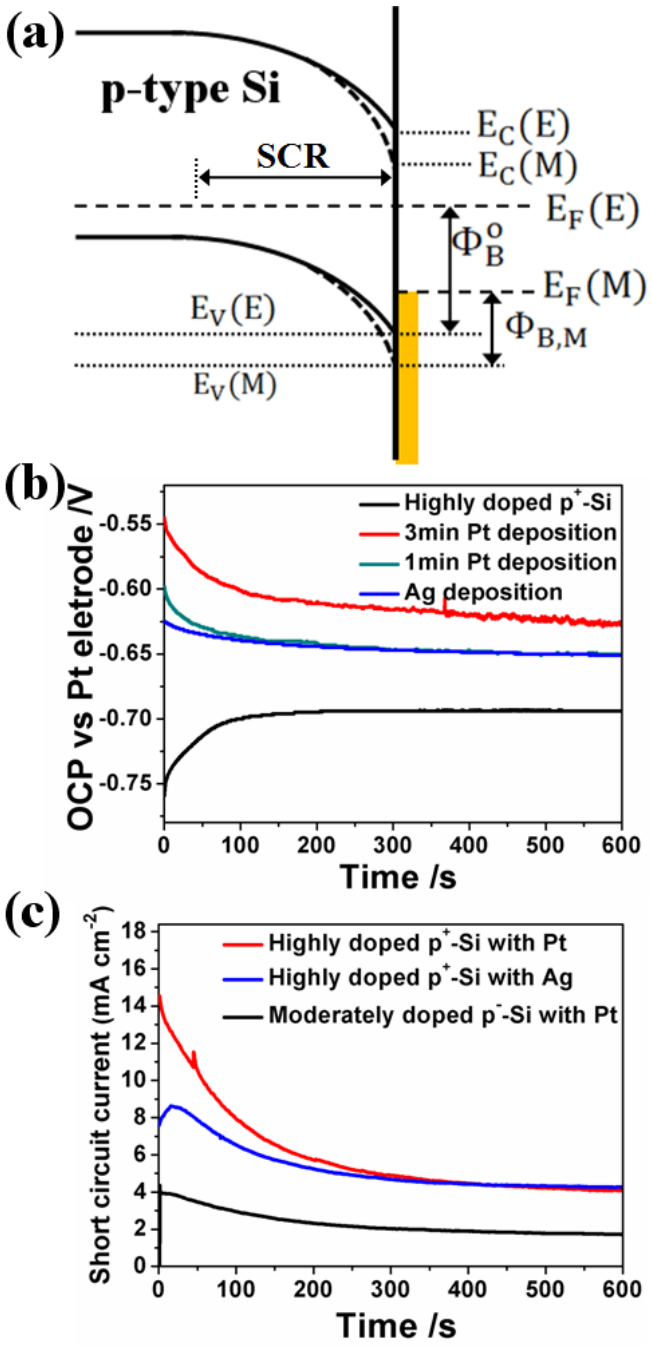
(a)
p-type Si
SCR
$E_C(E)$
$E_C(M)$
$E_F(E)$
Φ_B^o
$E_F(M)$
$E_V(E)$
$\Phi_{B,M}$
$E_V(M)$
(b)
OCP vs Pt eletrode /V
-0.55
-0.60
-0.65
-0.70
-0.75
0
100
200
300
400
500
600
Time /s
Highly doped p+-Si
3min Pt deposition
1min Pt deposition
Ag deposition
(c)
Short circuit current (mA cm-2)
18
16
14
12
10
8
6
4
2
0
0
100
200
300
400
500
600
Time /s
Highly doped p+-Si with Pt
Highly doped p+-Si with Ag
Moderately doped p--Si with Pt

Fig. 2